Tunable Lumped Components with Applications to Reconfigurable MEMS Filters

Dimitrios Peroulis, Sergio Pacheco, Kamal Sarabandi, and Linda P. B. Katehi,
Radiation Laboratory, Electrical Engineering and Computer Science Department,
University of Michigan, 1301 Beal Ave., Ann Arbor, MI 48109-2122

Abstract— **This paper presents a novel design scheme for tunable coplanar waveguide components with applications to compact lumped-element MEMS reconfigurable filters. Shunt MEMS switches are employed for tuning the values of lumped components frequently encountered in microwave integrated circuits. In particular, shunt capacitors, series inductors and shunt inductive stubs are the main tunable circuit elements utilized in this work. Furthermore, accurate equivalent circuits that include the most important parasitics introduced by the tuning mechanism are provided. Finally, the proposed method is applied to the design and implementation of very compact low-pass and bandpass tunable filters. The very high tunability range, the compactness of the resulting networks and their very wideband response constitute the main advantages of this technique.**

I. Introduction

RECENTLY there has been a growing interest in microelectromechanical (MEMS) components and their applications in microwave integrated circuits and antennas. MEMS based devices offer superior performance compared to their solid-state counterparts since they exhibit lower insertion loss and negligible power consumption and intermodulation distortion. It has already been demonstrated that MEMS devices can be successfully incorporated in high-isolation switching networks [1], [2], analog and digital phase shifters [3], [4] and reconfigurable antennas [5], [6]. However, little information is available on tunable circuits design methods.

In this paper a new technique of using MEMS switches for tuning lumped elements and its potential in reconfigurable compact filter design is illustrated. The main purpose of this work is twofold : First to demonstrate a design method for tunable circuits and, second, to investigate its capabilities and limitations of designing MEMS lumped-element tunable filters.

II. Tunable CPW-Based Lumped Components

In designing lumped-element circuits, capacitors and inductors in both series and shunt configurations, as well as combinations of those are needed. Several techniques are known for implementing these components. For example, shunt or series metal-insulator-metal (MIM) capacitors can be readily employed, and spiral inductors or stubs are well-known choices for the inductive elements. On the other hand, none of these realizations can be easily utilized for directly tuning the values of the filter components. Therefore, other methods should be used instead.

A. Tunable Shunt Capacitors

A conceptually easy way to implement a tunable capacitor is to use a capacitive MEMS switch. For example, a metallic plate suspended over a cpw line that can be electrostatically actuated and short the line is a well-known technique [7]. The switch in the up state presents a very small capacitance (typically in the order of 20 to 50 fF), while the down state capacitance is in the range of 1 to 4 pF. Therefore, a tuning range of 40 to 80 can be achieved. While this simplistic model of a capacitive MEMS switch may be adequate for switching-network design, it is not sufficient for filter design due to the parasitic components that cannot be neglected in the latter case.

Although a switch that has already been reported [8] is used in this work as a vehicle to demonstrate the previous concepts, the techniques that will follow can be readily applied to most of the capacitive switches with similar properties. This shunt switch is fabricated over a cpw line and has three movable plates, one over each conductor of the cpw (Fig. 1). Fig. 1a illustrates the layout of this switch in a configuration that will be later used for the filter implementation. Fig. 1b shows a lumped-element equivalent T-network that can be used to accurately simulate the RF performance of this switch.
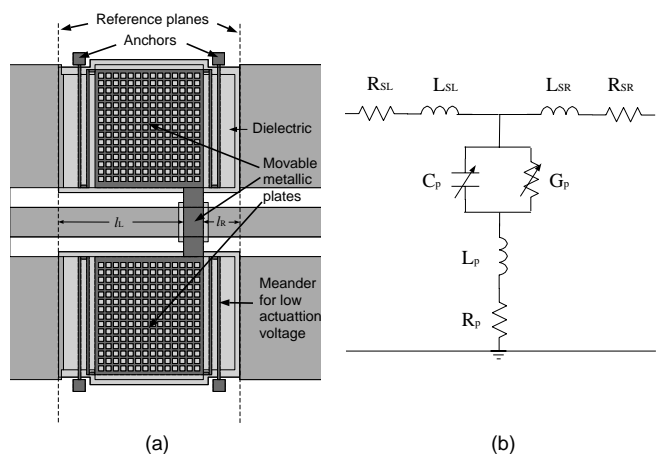

Fig. 1. (a) Capacitive MEMS switch used as tunable capacitor over a cpw line, and (b) its equivalent circuit.

The capacitance C_p is given by the series connection of the capacitance C_{ct} and C_{gnd}, where C_{ct} (C_{gnd}) is the capacitance formed between the center conductor (ground plane) of the cpw and the plate on top of it. As can be seen in Fig. 1a, access holes have been introduced in the

plates on top of the ground planes to allow faster operation by reducing the air-damping effect underneath the plate. Although this does reduce the corresponding capacitance, C_{gnd} remains much larger than C_{ct} and therefore $C_p \simeq C_{ct}$ for the geometry of Fig. 1a. This fact will be true for all the switches that will be presented in this paper. Following [9], the up and down-state capacitances can be expressed as

$$C_p = \begin{cases} \varepsilon_0 \frac{A}{d+t_d/\varepsilon_r} + C_{frng} & : \quad \text{up-state} \\ \varepsilon_0 \varepsilon_r \frac{A}{t_d+t_{rough}} & : \quad \text{down-state} \end{cases} \quad (1)$$

where A is the plate area on top of the center conductor, d is the distance between the switch and the cpw in the up-state ($d \simeq 3\mu m$ for the switches in this work), t_d is the thickness of the dielectric material on top of the cpw line ($t_d = 1200\mathring{A}$), ε_r is the dielectric constant of the material used ($\varepsilon_r \simeq 7.5$ for PECVD Si_3N_4) and C_{frng} is the additional capacitance due to the fringing field effect. Finally, t_{rough} is an effective thickness that takes roughness into account. For the geometry shown in Fig. 1a, the extracted up and down capacitances from the measured S-parameters are $C_p^{up} = 17$ fF and $C_p^{down} = 920$ fF.

R_p and L_p represent the resistance and inductance of the switch beam and can be modeled with a full wave simulator. Typical values range from 0.1–2 Ω and 1–60 pH for the R_p and L_p respectively. They are primarily dominated by the beams connecting the switch plates [2]. G_p depends on the quality of the dielectric material and can be readily modeled using the formula:

$$G_p = \begin{cases} 0 & : \quad \text{up-state} \\ \omega C_p \tan\delta & : \quad \text{down-state} \end{cases} \quad (2)$$

where $\tan\delta$ is the loss factor of the dielectric material used as the insulator. The inductive sections L_{SL} and L_{SR} are used to model the short transmission line sections of lengths l_L and l_R respectively (see Fig. 1). These inductances are important since their values can be comparable to those of the inductors used in the filter. L_{SL} can be approximated as :

$$L_{SL} \simeq \frac{2Z_0}{\omega} \tan(\beta l_L/2) \simeq Z_0 \beta l_L / \omega \quad (3)$$

A similar formula holds for L_{SR}. The resistances R_{SL} and R_{SR} represent the ohmic loss of the same transmission line sections and can be modeled as:

$$R_{SL} \simeq 2\alpha Z_0 l_L \quad \text{and} \quad R_{SR} \simeq 2\alpha Z_0 l_R \quad (4)$$

where α is the measured attenuation of the transmission line (approximately 1.2 dB/cm for the circuits measured in this work).

B. Tunable Series Inductor

It is a well-known fact that a relatively high-Q inductor can be implemented with a short section of a transmission line assuming that the length is less than approximately a tenth of a wavelength (Fig. 2). The component values of this equivalent circuit can be calculated by formulas similar
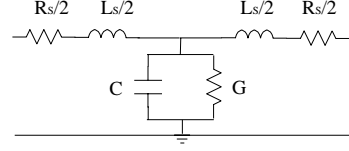

Fig. 2. Equivalent circuit of a short transmission line

to the ones given in (2),(3),(4). The quality factor of this inductor can be estimated if the small shunt capacitance and conductance are neglected, as follows :

$$Q_{S,ind} = \frac{\omega L_S}{R_S} = \frac{\tan(\beta l/2)}{\alpha l} \simeq \frac{\beta}{2\alpha} \quad (5)$$

This equation results in a quality factor of 19 at 10 GHz with a measured attenuation of 1.2 dB/cm.

The reconfigurability of this element can be achieved in association with the tunable capacitor. An example that explains this idea is illustrated in Fig. 3, which shows a short transmission line with four capacitive MEMS switches numbered from one to four. Assuming that 1) the
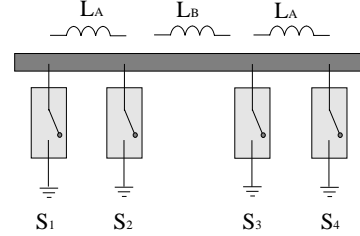

Fig. 3. Tunable series inductor with four switches.

up-state capacitance is negligible, and 2) all four switches are identical, the series inductor can be tuned by actuating different sets of switches. For instance, if S_1 and S_4 are down, then the inductance value between these switches is $L_{ind}^{1,4} = L_B + 2L_A + 3(L_{SL} + L_{SR})$. On the other hand, when S_2 and S_3 are down, this value becomes $L_{ind}^{2,3} = L_B + L_{SL} + L_{SR}$ resulting in a tuning ratio of:

$$\mathcal{R}_{ind} \equiv \frac{L_B + 2L_A + 3(L_{SL} + L_{SR})}{L_B + L_{SL} + L_{SR}} = 1+2\frac{L_A + L_{SL} + L_{SR}}{L_B + L_{SL} + L_{SR}} \quad (6)$$

As a result the tuning ratio can be quite high and is totally controlled by the placement of the switches. Moreover, more switching pairs can be used and the inductor can take more discrete values between $L_{SL} + L_{SR}$ and $L_B + 2L_A + 3(L_{SL} + L_{SR})$. Obviously different design schemes can also be used with either the same or other type of switches that will result in different tuning ranges.

C. Tunable Shunt Inductor

An inductive cpw stub is usually employed to implement a shunt resonator. Although stubs as long as $\lambda/4$ have been used, only short stubs are discussed in this work. Such short inductive stubs exhibit similar properties (in phase shifting and quality factor) to the series inductors presented in the previous subsection. Therefore, their equivalent circuits are not substantially different from the ones already presented and will not be repeated.

A metallic plate suspended on top of the inductor and the ground plane as shown in Fig. 4a can be utilized for tuning this component. The plate covers completely the inductive stub and a part of the ground plane. Furthermore, the holes have been removed from the plate just above the stub in order to achieve a higher capacitance (for clarity in the figure, the metallic plate is transparent). In the up-state, the plate should not substantially affect the value of the inductance. In the down-state, however, the stub is effectively shorted by the capacitively formed RF short and the inductance value changes to an effective inductance L_{eff}.
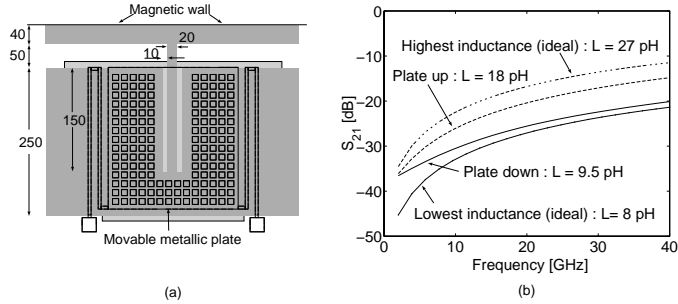

Fig. 4. (a) Tunable shunt inductor (dimensions are in μm). (b) Simulated response.

IE3D [10] was used to model the inductance in the up and down position and demonstrate this concept. The simulated results are presented in Fig. 4b, which clearly indicate that a tuning range of approximately 2:1 can be realized through this technique. Two ideal inductance values are also mentioned in Fig. 4, which correspond to the inductances that could be realized if it was possible to perfectly short the stub in the down state and leave it unaffected in the up state. Obviously, an even higher tuning range could be achieved if these minimum and maximum inductance values could be obtained. A metal-to-metal contact switch could, therefore, provide results closer to the ideal situation. Additionally, the tuning range can be further optimized by changing the geometrical features of the stub.

III. APPLICATIONS, MEASUREMENTS AND DISCUSSION

The tunable components analyzed in the previous section can be combined to form potentially useful tunable circuits. To demonstrate this concept, two tunable filters were implemented using these ideas. The fabrication process of the MEMS switch utilized in this circuits can be found in [8] and is not repeated here.

A. Low-pass Filter

The tunable low-pass filter is presented in Fig. 5. The filter's bandwidth is 10 GHz when switches 1 and 5 are activated and 30 GHz when 2, 3 and 4 are active. Therefore, a tuning range of 3:1 is obtained. Simplified equivalent circuits for the two states are presented in Fig. 5b. The design in both states is based on the classical Chebyshev low-pass prototype and it constitutes a direct application of the tunable capacitor and series inductor design presented in the previous section. It is also easy to see that the filter
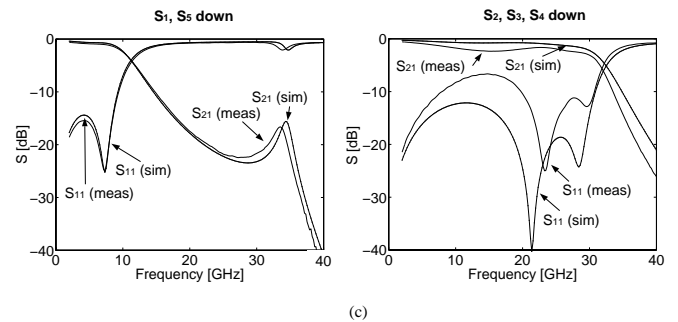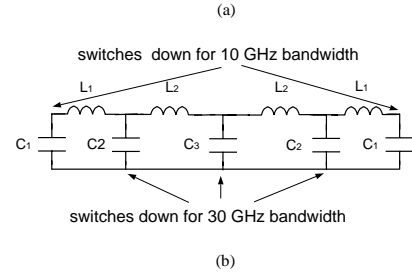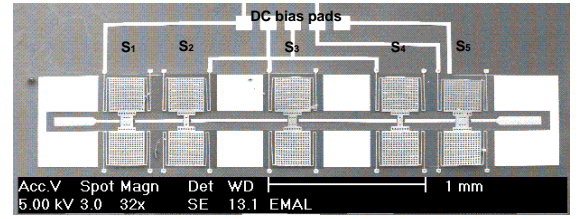

Fig. 5. (a) Low-pass filter. (b) Simplified equivalent circuit. (c) Simulated and measured response.

has 3(5) poles when the cut-off frequency is at 10GHz (30 GHz).

The filter's insertion loss is approximately 1.1 dB at the 10 GHz-bandwidth operation with a return loss of less than -15 dB. However, there is a small increase of 0.8 dB in the insertion loss at the 30 GHz band. This is due to the increased return loss at the level of -8 dB around 20 GHz. This discrepancy can be attributed to the somewhat higher capacitances that were obtained when the switches 2, 3 and 4 were down. One more iteration would tune these capacitor values and result in an optimized design.

B. Band-pass Filter

The tunable bandpass filter design is less straightforward than the low-pass design due to the presence of the small inductors L_{SL} and L_{SR}, which cause the classical LC resonator to substantially deviate from the ideal case. In addition, such a scheme is very hard to be made tunable. Instead a new circuit is proposed, which is illustrated in Fig. 6. Such a design can be fully reconfigurable since all the elements can be tuned as discussed in Section II. Therefore it is possible to move the resonant frequency without affecting the absolute bandwidth of the filter.

The frequency response of the circuit in Fig. 6b can be readily obtained by means of an even-odd mode analysis.
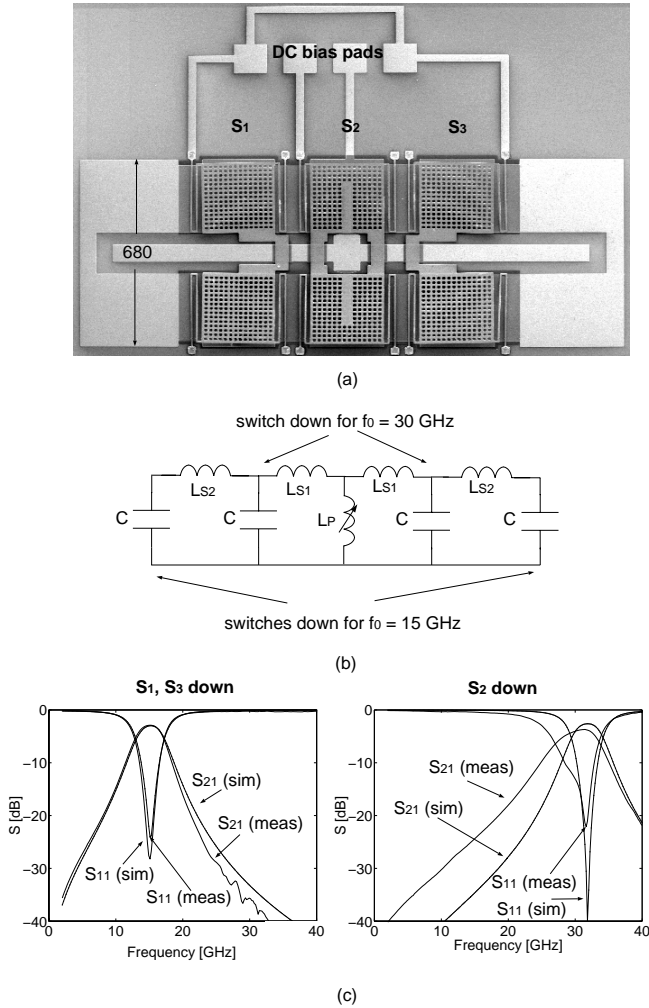
Fig. 6. (a) Band-pass filter (dimensions are in μm). (b) Simplified equivalent circuit. (c) Simulated and measured response.

This analysis shows that this filter has two double poles at

$$f_{pe} = \frac{1}{2\pi\sqrt{C(L_s + 2L_p)}} \quad \text{and} \quad f_{po} = \frac{1}{2\pi\sqrt{CL_s}} \qquad (7)$$

three zeros at infinity and a zero at s=0. L_S is $L_{S1} + L_{S2}$ (L_{S1}) when the center switch is up (down) and the others are down (up). The full frequency response is given by

$$S_{21} = \frac{s\frac{\omega_0}{Q}\left(\omega_{0o}^2 - \omega_{0e}^2\right)}{\left(s^2 + s\frac{\omega_{0e}}{Q_e} + \omega_{0e}^2\right)\left(s^2 + s\frac{\omega_{0o}}{Q_o} + \omega_{0o}^2\right)} \qquad (8)$$

where the quality factors are as follows:

$$Q_e = Z_0\sqrt{\frac{C}{L_s + 2L_p}} \quad \text{and} \quad Q_0 = Z_0\sqrt{\frac{C}{L_s}} \qquad (9)$$

and $\omega_{0o}/Q_o = \omega_{0e}/Q_e = \omega_0/Q = 1/CZ_0$

Based on the above equations, a bandpass filter with a tunable center frequency at 15 and 30 GHz was designed. Fig. 6c presents the theoretical and measured results for the two states. We first observe that the results of the lower frequency filter agree favorably with the theoretical modeling. Both the center frequency and the bandwidth, as well as the insertion and return loss are correctly predicted from the theory. Nevertheless, this is not the case for the filter around 30 GHz since there is a considerable distortion compared to the modeling. The reason for this discrepancy lies on the fact that the tuning range of the shunt inductor is smaller that the one predicted by the theory. The results can be improved if a metal-to-metal contact switch is used to tune the shunt inductor, especially for lower frequency designs. Finally, it is worth noticing that the total area of this 4th order tunable filter is less than 1mm^2.

IV. Conclusions

We have demonstrated a new design scheme for tuning many circuit elements using MEMS switches. Accurate lumped element equivalent circuits have been provided for these elements and the main salient features have been demonstrated. Reconfigurable circuits that follow the proposed techniques tend to be relatively simple, ultra compact and very wideband. This technique has been applied to the design of novel low-pass and bandpass filters that have demonstrated a very high tuning range. Overall, this technique has the potential to be applied to many classes of networks where compact, wideband, tunable lumped-element components are required.

Acknowledgments

References

[1] J. B. Muldavin, G. M. Rebeiz, *High-Isolation CPW MEMS Shunt Switches – Part 2: Design*, IEEE Transactions on Microwave Theory and Techniques, Vol. 48, no. 6, June 2000, pp. 1053-1056.

[2] D. Peroulis, S. Pacheco, K. Sarabandi, L.P.B. Katehi, *MEMS devices for High Isolation Switching and Tunable Filtering*, IEEE International Microwave Symposium Digest, Vol.2, June 2000, pp. 1217-1220.

[3] N. S. Barker, *Distributed MEMS Transmission Lines*, Ph.D. Dissertation, University of Michigan, 1999.

[4] J. S. Hayden, G. M. Rebeiz, *One and Two-Bit Low-Loss Cascadable MEMS Distributed X-Band Phase Shifters*, IEEE International Microwave Symposium Digest, Vol.2, June 2000, pp. 161-164.

[5] J. C. Chiao, Y. Fu, J. M. Chio, M. DeLisio, L. Y. Lin, *MEMS Reconfigurable Antenna*, IEEE International Microwave Symposium Digest, Vol.2, June 1999, pp. 1515-1518.

[6] C. Bozler, R. Drangmeister, S. Duffy, M. Gouker, J. Knecht, *MEMS Microswitch Arrays for Reconfigurable Distributed Microwave Components*, IEEE International Microwave Symposium Digest, Vol.2, June 2000, pp. 153-160.

[7] C. Goldsmith, J. Randall, S. Eshelman, T. H. Lin, D. Denniston, S. Chen, B. Norvell, *Characteristics of Micromachined Switches at Microwave Frequencies*, IEEE International Microwave Symposium Digest, Vol.2, June 1996, pp. 1141-1144.

[8] S. Pacheco, L. P. B. Katehi, C. T. Nguyen, *Design of Low Actuation Voltage RF MEMS Switch*, ,IEEE International Microwave Symposium Digest, Vol.1, June 2000, pp. 165-168.

[9] J. B. Muldavin, G. M. Rebeiz, *High-Isolation CPW MEMS Shunt Switches – Part 1: Modeling*, IEEE Transactions on Microwave Theory and Techniques, Vol. 48, no. 6, June 2000, pp. 1045-1052.

[10] Zeland's IE3D, Release 7, 2000.